Efficient Hydrogenation

DOI: 10.1002/ange.200600359

Single-Step Conversion of Dimethyl Terephthalate into Cyclohexanedimethanol with Ru_5PtSn, a Trimetallic Nanoparticle Catalyst**

Ana B. Hungria, Robert Raja, Richard D. Adams, Burjor Captain, John Meurig Thomas,* Paul A. Midgley, Vladimir Golovko, and Brian F. G. Johnson*

As a linker molecule in the polymer industry, 1,4-cyclohexanedimethanol (CHDM) is a highly valued and extensively used reagent.[1] It is, for example, preferred[2] over ethylene glycol as a stepping stone in the production of polyester fibers for applications involving polycarbonates and polyurethanes.[1,3] Industrially, CHDM is prepared by a two-step process using two reactors.[1,4] The first step is the highly exothermic conversion of dimethyl terephthalate (DMT) into dimethyl hexahydroterephthalate (DMHT) by using a supported Pd catalyst in the temperature range of 160–180 °C and an H_2 pressure of 30–48 MPa (300–480 bar). The intermediate DMHT is then converted into CHDM by using a copper–chromite catalyst at temperatures about 200 °C and an H_2 pressure of about 40 bar.[4] We have already shown that bimetallic nanoparticle catalysts,[5] such as (silica-supported) Ru_5Pt, $Ru_{10}Pt_2$, Ru_6Pd_6, and $Ru_{12}Cu_4$, can promote the single-step conversion of DMT into CHDM and are more efficient than the Angelici-type catalyst,[6] which consists of a rhodium complex tethered on silica-supported palladium. Herein, we report that of the wide range of possible hydrogenation products of DMT (Scheme 1) mainly the desired products DMHT and CHDM are formed with supported nanoparticles of the trimetallic cluster Ru_5PtSn. This catalyst shows both the highest activity and selectivity yet observed in any single-step conversion of DMT into CHDM under mild conditions (100 °C, 20 bar H_2).

The parent material, $[PtRu_5(CO)_{15}(\mu\text{-}SnPh_2)(\mu_6\text{-}C)]$ (**1**; Figure 1),[7] was obtained from the reaction of Ph_3SnH with the hexanuclear bimetallic complex $[PtRu_5(CO)_{16}(\mu_6\text{-}C)]$.[8] For comparison, we also carried out a few experiments (see below) using $[PtRu_5(CO)_{15}(\mu\text{-}GePh_2)(\mu_6\text{-}C)]$ (**2**) prepared from the same hexanuclear complex and Ph_3GeH. The heterotrinuclear (Ru-Pt-Sn) complex was anchored onto a mesoporous silica (Davison 38 Å) through silanol groups, as described previously.[5a,9] The reaction conditions and the results for the hydrogenation of DMT are presented in Table 1. From these data and from Figure 2, the superior performance of the trimetallic nanoparticle catalyst is clear. This is not surprising in view of the well-known role of tin as a modifier in bimetallic petroleum-reforming catalysts.[10] It has also been shown that Pt enhances the activity of RuSn catalysts for the hydrogenation of 1,4-cyclohexanedicarboxylic acid to CHDM.[11]

The significant improvement in performance[9a] that tin effects to bimetallic catalysts is also relevant here. In previous studies, EXAFS measurements showed that the tin atom serves to anchor the metal clusters firmly to the siliceous supports.[12] Similar measurements (now underway) are needed to shed light on the dramatic difference in behavior between Ru_5PtSn and Ru_5PtGe, but we can say right away that it was extremely difficult to anchor the germanium parent **2** onto the silica under the same conditions for which **1** became firmly attached. Both Sn^{IV} and Ge^{IV} are well-known[13,14] to be able to replace tetrahedrally coordinated Si^{IV} ions in open-framework solids. However, in this work, only infinitesimal quantities of Ge could be detected by electron-induced X-ray emission. We believe that it is more difficult to attach Ge to the siliceous surface because it is more difficult to cleave Ge–C bonds than Sn–C bonds in the EPh_2 ligands of the precursors **1** and **2**, respectively.

High-angle annular-dark-field (HAADF) examination[15] of the monodispersed trimetallic catalysts showed high

[*] Prof. Dr. R. D. Adams, Dr. B. Captain
Department of Chemistry and Biochemistry
University of South Carolina
Columbia, SC 29208 (USA)
Fax: (+1) 803-777-6781
E-mail: adams@mail.chem.sc.edu
Dr. A. B. Hungria, Prof. J. M. Thomas, Dr. P. A. Midgley
Department of Materials Science
University of Cambridge
Cambridge, CB2 3QZ (UK)
Fax: (+44) 1223-334-563
E-mail: jmt2@cam.ac.uk
Dr. R. Raja, Dr. V. Golovko, Prof. B. F. G. Johnson
University Chemical Laboratory
University of Cambridge
Cambridge, CB2 1EW (UK)

[**] This research was supported by the Office of Basic Energy Sciences of the US Department of Energy under Grant No. DE-FG02-00ER14980.

Supporting information for this article is available on the WWW under http://www.angewandte.org or from the author.

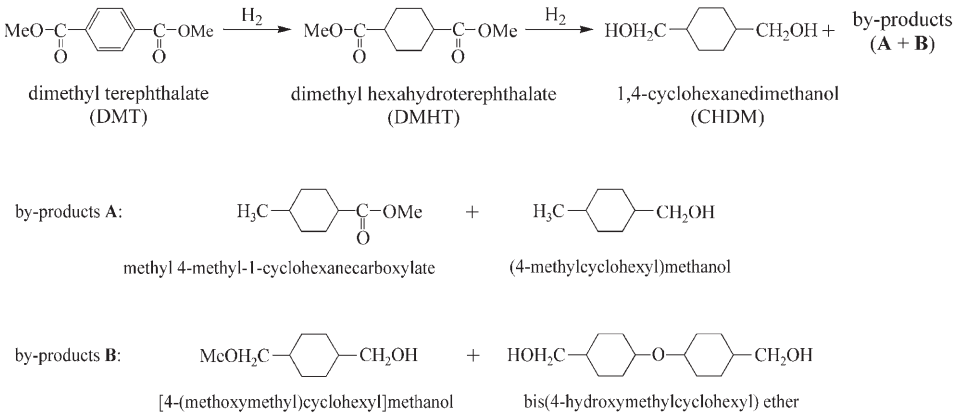

Scheme 1. Possible hydrogenation products of DMT.

dispersion on the supports both before and after catalysis (Figure 3). There was clearly no sintering of the nanoparticles during the exothermic hydrogenation reaction. Moreover, extremely localized nanoanalysis—by electron-induced X-ray emission (Figure 4)—showed that the composition of individual particles (volumes of ca. 1 nm^3 analyzed) is very close to the stoichiometry Ru_5PtSn of the precursor **1**.

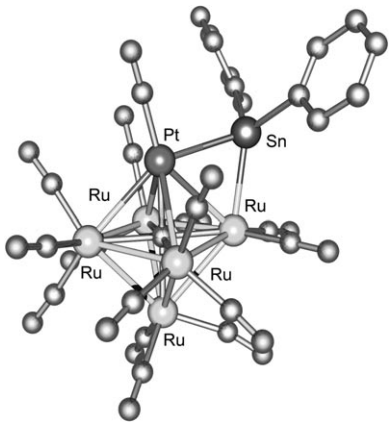

Figure 1. Molecular structure of complex **1**.

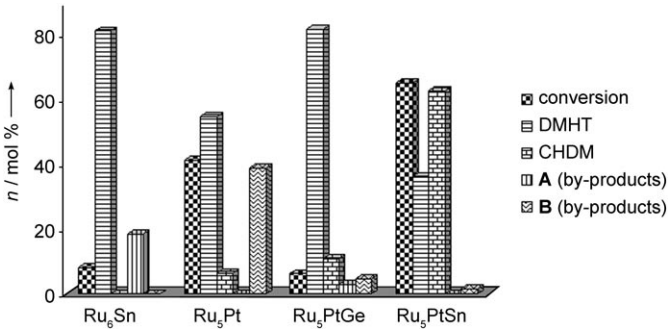

Figure 2. Bar chart comparing the activity and selectivity of the Ru_5PtSn catalyst with those of other bi- and trimetallic catalysts for the hydrogenation of DMT. H_2 pressure: 20 bar; $T = 373$ K; $t = 24$ h. See Table 1 and Experimental Section for further details.

HAADF tomography has been successfully applied before to explore the spatial distribution and morphology of supported nanoparticles.[5,16] With this purpose, a series of *Z*-contrast (Z = atomic number) images of the Ru_5PtSn catalyst was acquired every 2° between −70° and 70°. Figure 5 shows the axial projection of a specimen tomogram together with a series of single slices through the tomogram, from which a tendency of the particles to be evenly distributed mainly close to the surface of the material can be observed. In certain slices (Figures 5b and c) there are some zones with a greater density of particles inside the volume of the material. (A movie showing the tomographic retrieval of the interior distribution of the trimetallic nanoparticle catalysts is provided in the Supporting Information.)

In summary, we have discovered the synergistic value of the

Table 1: Comparison of catalysts for the hydrogenation of DMT.[a]

Catalyst	t [h]	T [K]	Conv. [mol%]	TOF[b] [h^{-1}]	Product distribution [mol%] DMHT	CHDM	A	B
Ru_5PtSn/SiO_2	4	373	16.8	247	54.7	45.2	–	–
	8	373	36.5	278	41.5	57.5	–	0.9
	24	373	64.9	242	36.2	62.5	–	1.5
Ru_5PtSn/SiO_2	8	393	45.4	339	34.9	60.0	–	5.0
	24	393	76.6	290	29.7	45.1	8.9	16.4
Ru_5PtSn/SiO_2	8	413	61.2	376	30.3	43.9	9.9	15.8
Ru_5PtSn/SiO_2[c]	8	393	63.9	387	9.5	71.2	8.3	11.2
Ru_5PtGe/SiO_2	4	373	2.2	19	85.0	10.2	2.2	2.5
	8	373	4.1	35	83.3	10.5	2.5	3.7
	24	373	6.2	22	81.5	10.8	2.9	4.7
Ru_5Pt/SiO_2	4	373	6.8	148	55.3	31.9	–	12.7
	8	373	21.2	198	51.2	11.5	–	37.2
	24	373	41.3	145	54.6	6.5	–	38.8
Ru_6Sn/SiO_2[d]	4	373	–	–	–	–	–	–
	8	373	5.3	54	77.2	–	22.6	–
	24	373	8.0	27	81.0	–	18.6	–

[a] Conditions, unless otherwise given: SiO_2: mesoporous Davison silica with a pore diameter of 38 Å; H_2 pressure: 20 bar. [b] $TOF = [(mol_{substr})(mol_{cluster})^{-1} h^{-1}]$. [c] H_2 pressure: 40 bar. [d] Mesoporous SiO_2 of the MCM-41 type.

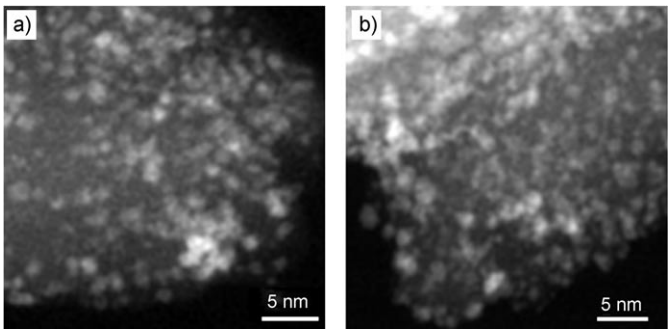

Figure 3. HAADF images of Ru_5PtSn nanoclusters on Davison 38 Å silica before (a) and after (b) catalysis.

trimetallic nanoparticle catalyst Ru_5PtSn as a highly efficient and selective means of effecting the catalytic single-step hydrogenation of DMT to CHDM under mild conditions. The presence of tin in the nanoparticle catalyst appears to play a key role in anchoring the particle owing to its oxophilicity for the support, which in turn diminishes the tendency for the nanoparticles to sinter.

Experimental Section

The organometallic complexes **1** and **2** were prepared according to a published procedure.[7] The catalysts were prepared following standard procedures reported earlier.[5a,9] Rather than employing as porous support the popular (organic-template-derived) MCM-type (which have non-intersecting pores) and related silicas such as SBA-15, we used a commercially available (from Grace Davison) desiccant silica with a narrow pore-size distribution (designated Davison 923; pore diameter 38 Å). This support is made by reacting sodium silicate with a strong mineral acid (usually sulfuric acid); the pore size is controlled by gel time, final pH value, temperature, concentration of reactants, etc. Compared to MCM-41 type silica, the Davison silica is much lower in cost, thermally and mechanically more stable, and less susceptible to structural collapse. It also has some intersecting pores that facilitate the diffusion of the reactant species to the immobilized catalyst, and its surface area is close to 700 $m^2 g^{-1}$.

A slurry of cluster **1** or **2** (100 mg) in dichloromethane (20 mL) and diethyl ether (20 mL) was added under inert atmosphere (Ar) to 400 mg of thoroughly degassed mesoporous silica Davison 923. The mixture was stirred for 12 h. The support with the adsorbed cluster was allowed to settle and the liquid (on top) was removed. The support (with the anchored cluster) was washed twice with diethyl ether (20 mL) and dried in vacuum. The catalyst was activated (decarbonylated) by calcination in vacuum at ca. 200 °C for 2 h. The loading of the clusters on the mesoporous support varied from sample to sample; it was accurately determined by inductively coupled plasma (ICP) analysis for each catalytic experiment. For the Ru_5PtSn cluster, the loadings on the support varied from 0.0015 to 0.0026 mmol, whereas for the Ru_5PtGe cluster the loadings were in the range of 0.00165 to 0.00372 mmol.

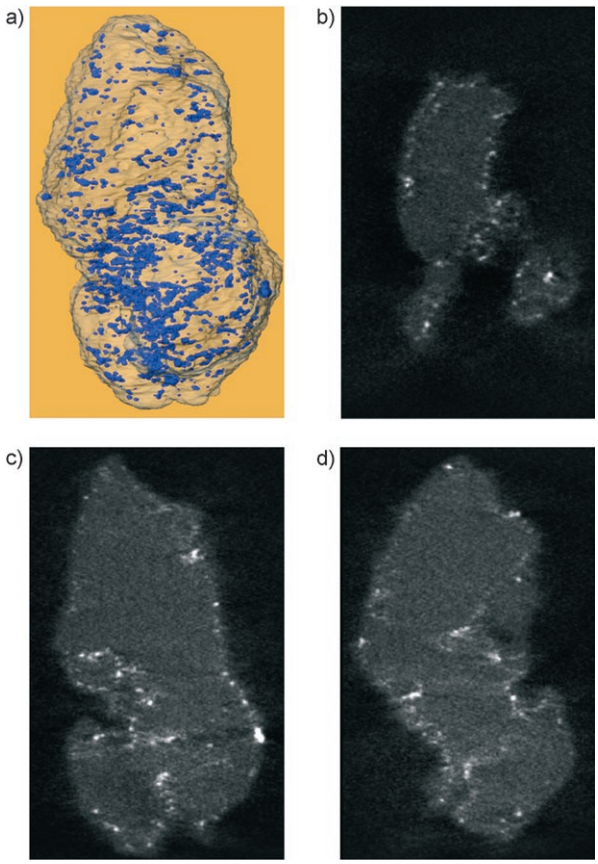

Figure 5. Axial projection of a specimen tomogram (a), with successive slices (b–d) through a scanning electron tomogram of Ru_5PtSn supported on Davison 38 Å silica. See Supporting Information for a video of the full dynamic tomogram.

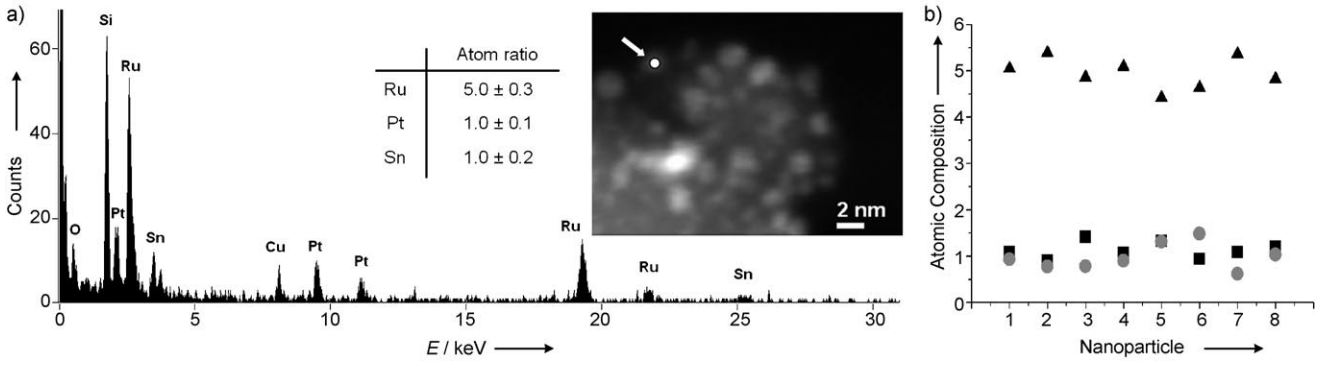

Figure 4. a) Electron-induced X-ray emission spectrum of nanoparticles of Ru_5PtSn nanoclusters on Davison 38 Å silica. The arrow in the inset points to the particle for which this emission spectrum was recorded. The peak for Cu in this spectrum originates from the sample holder. b) Plot showing the uniformity of the composition of several nanoparticles of the Ru_5PtSn catalyst: triangles Ru; circles Sn; squares Pt.

Electron microscopy: For the tomograms shown in Figure 5, 71 images were recorded with an acquisition time of 20 s every 2° from +70° to −70° using a Fischione ultrahigh-tilt tomography holder model 2020 and a FEI Tecnai F20 field emission gun transmission electron microscope operated at 200 kV in scanning transmission electron microscope (STEM) mode. The probe size was approximately 0.5 nm in diameter, and each HAADF image was recorded with a pixel size of 0.27 nm using a Fischione HAADF detector. The "missing wedge" of data (at high tilts) leads to anisotropic spatial resolution, with a degradation of resolution in the direction parallel to the optical axis of about 30%. Image acquisition was undertaken using the FEI software package Xplore3D. Images were then aligned sequentially using Inspect 3D. Reconstructions, again with Inspect 3D, were performed using either weighted back-projection (WBP) routines or an iterative routine (SIRT) that constrains the reconstructed volume to match the original images when re-projected back along the original tilt directions. This constraint has the effect of minimizing some of the unwanted effects of the limited data sampling and greatly reduces the "fan" artifact that can be evident in many WBP reconstructions. Voxel projections were constructed in Inspect 3D, and surface rendering (after a segmentation process) was undertaken using Amira software.

Catalysis: The liquid-phase hydrogenation of DMT was carried out in a high-pressure, teflon-lined, stainless steel catalytic reactor (150 mL). The catalyst (50 mg), which was stored under inert conditions (Ar), was transferred to the reactor (using a robotically controlled catalyst-delivery unit) containing about 2.5 g of DMT (Aldrich, ≥99% pure) dissolved in ethanol (75 mL) and 0.5 g of the internal standard (hexadecane). The reactor was sealed, and its contents were inertized (thrice) with dry N_2 prior to reaction. The contents of the reactor were stirred (1700 rpm) and heated to the desired temperature (from a low of 373 K to a high of 413 K). Dry hydrogen (dynamic pressure of 20 or 40 bar, see Table 1) was pressurized into the reaction vessel and, using mini-robot liquid- and gas-sampling valves, small aliquots (0.1 μL) of liquid and gas samples were removed to study the kinetics of the reaction without perturbing the pressure in the reactor.

The composition of the liquid and gaseous products was continuously monitored by using an online computer-controlled system linked to a GC and LC-MS system (Shimadzu QP 8000). The products were analyzed (using hexadecane as the internal standard) by gas chromatography (Varian, Model 3400 CX) employing an HP-1 capillary column (25 m × 0.32 mm) and a flame ionization detector. The identities of the products were first confirmed using authenticated standards, and their individual response factors were determined by using a suitable internal standard (calibration method). The conversions (Conv.) and selectivities (Sel.) were determined as defined by Equations (1) and (2), and the yields were normalized

$$\text{Conv. } [\%] = \frac{\text{mol}_{\text{substrate (initial)}} - \text{mol}_{\text{substrate (residual)}}}{\text{mol}_{\text{substrate (initial)}}} \times 100 \quad (1)$$

$$\text{Sel. } [\%] = \frac{\text{mol}_{\text{individual product}}}{\text{mol}_{\text{total products}}} \times 100 \quad (2)$$

with respect to the response factors obtained as described above. For the internal-standard GC method, the response factor (RF) and mol% of individual products were calculated using Equations (3) and (4). The identity of the products was further confirmed by GC-MS.

$$\text{RF} = \frac{\text{mol}_{\text{product}}}{\text{mol}_{\text{standard}}} \times \frac{\text{area}_{\text{standard}}}{\text{area}_{\text{product}}} \quad (3)$$

$$\text{mol}\,\%_{\text{product}} = \text{RF} \times \text{mol}_{\text{standard}} \times \frac{\text{area}_{\text{product}}}{\text{area}_{\text{standard}}} \times \frac{100}{\text{mol}_{\text{sample}}} \quad (4)$$

The Ru_5PtSn catalysts were reused three times without appreciable loss in catalytic activity or selectivity. Further experiments analogous to those reported earlier[5a] were carried out to rule out the possibility of leaching, and analysis of the resulting filtrate at the end of reaction (24 h) by ICP and AAS revealed only trace amounts (< 5 ppb) of dissolved metal ions (Pt, Ru, Sn).

Received: January 27, 2006
Revised: April 24, 2006
Published online: June 23, 2006

Keywords: electron microscopy · heterogeneous catalysis · hydrogenation · nanoparticles · tomography

[1] S. R. Turner, *Polym. Sci.* **2004**, *42*, 5847.
[2] B. J. Sublett, G. W. Connell (Eastman Chemical), US-A 5559159, **1995** [*Chem. Abstr.* **1996**, *125*, 277914v].
[3] R. R. Amborse, J. B. O'Dwyer, B. K. Johnston, D. P. Zielinski, S. Porter, W. H. Tyger (PPG Industries), US-A 4859743, **1988** [*Chem. Abstr.* **1990**, *112*, 38296v].
[4] a) M. L. Schlossman (Tevco), US-A 4301046, **1981** [*Chem. Abstr.* **1982**, *96*, 24664c]; b) P. Appleton, M. A. Wood (Eastman Chemical), US 5414159, **1993** [*Chem. Abstr.* **1995**, *123*, 170535d].
[5] a) R. Raja, T. Khimyak, J. M. Thomas, S. Hermans, B. F. G. Johnson, *Angew. Chem.* **2001**, *113*, 4774; *Angew. Chem. Int. Ed.* **2001**, *40*, 4638; b) J. M. Thomas, B. F. G. Johnson, R. Raja, G. Sankar, P. A. Midgley, *Acc. Chem. Res.* **2003**, *36*, 20.
[6] H. Yang, H. R. Gao, R. J. Angelici, *Organometallics* **2000**, *19*, 622.
[7] R. D. Adams, B. Captain, W. Fu, *J. Organomet. Chem.* **2003**, *671*, 158.
[8] R. D. Adams, W. Wu, *J. Cluster Sci.* **1991**, *2*, 271.
[9] a) S. Hermans, R. Raja, J. M. Thomas, B. F. G. Johnson, G. Sankar, D. Gleeson, *Angew. Chem.* **2001**, *113*, 1251; *Angew. Chem. Int. Ed.* **2001**, *40*, 1211; b) D. S. Shephard, T. Maschmeyer, G. Sankar, J. M. Thomas, D. Ozkaya, B. F. G. Johnson, R. Raja, R. D. Oldroyd, R. G. Bell, *Chem. Eur. J.* **1998**, *4*, 1214.
[10] a) R. Burch, *J. Catal.* **1981**, *71*, 348; b) R. Burch, L. C. Garla, *J. Catal.* **1981**, *71*, 360; c) R. Srinivasan, B. H. Davis, *Platinum Met. Rev.* **1992**, *36*, 151; d) T. Fujikawa, F. H. Ribeiro, G. A. Somorjai, *J. Catal.* **1998**, *178*, 58.
[11] Y. Hara, K. Endou, *Appl. Catal. A: General* **2003**, *239*, 181.
[12] a) B. F. G. Johnson, S. A. Raynor, D. B. Brown, D. S. Shephard, T. Mashmeyer, J. M. Thomas, S. Hermans, R. Raja, G. Sankar, *J. Mol. Catal. A* **2002**, *182–183*, 89; b) J. M. Thomas, R. Raja, G. Sankar, B. F. G. Johnson, D. W. Lewis, *Chem. Eur. J.* **2001**, *7*, 2973.
[13] R. M. Barrer in *Hydrothermal Chemistry of Zeolites*, Academic Press, London, **1982**.
[14] a) R. D. Oldroyd, J. M. Thomas, G. Sankar, *Chem. Commun.* **1997**, 2025; b) R. D. Oldroyd, G. Sankar, J. M. Thomas, D. Ozkaya, *J. Phys. Chem. B* **1998**, *102*, 1849; c) J. M. Thomas, G. Sankar, M. C. Klunduk, M. P. Attfield, T. Maschmeyer, B. F. G. Johnson, R. G. Bell, *J. Phys. Chem. B* **1999**, *103*, 8809.
[15] a) D. Ozkaya, W. Z. Zhou, J. M. Thomas, P. Midgley, V. J. Keast, S. Hermans, *Catal. Lett.* **1999**, *60*, 113; b) J. M. Thomas, P. A. Midgley, *Chem. Commun.* **2004**, 1253.
[16] a) P. A. Midgley, M. Weyland, J. M. Thomas, P. L. Gai, E. D. Boyes, *Angew. Chem.* **2002**, *114*, 3958; *Angew. Chem. Int. Ed.* **2002**, *41*, 3804; b) J. M. Thomas, P. A. Midgley, T. J. Yates, J. S. Barnard, R. Raja, I. Arslan, M. Weyland, *Angew. Chem.* **2004**, *116*, 6913; *Angew. Chem. Int. Ed.* **2004**, *43*, 6745.

